Supported Faceted Gold Nanoparticles with Tunable Surface Plasmon Resonance for NIR-SERS

Giuseppe V. Bianco, Maria M. Giangregorio, Maria Losurdo, Pio Capezzuto, and Giovanni Bruno**

A novel dry plasma methodology for fabricating directly stabilized substrate-supported gold nanoparticle (NP) ensembles for near infrared surface enhanced Raman scattering (NIR SERS) is presented. This maskless stepwise growth exploits Au-sulfide seeds by plasma sulfidization of gold nuclei to produce highly faceted Au NPs with a multiple plasmon resonance that can be tuned from the visible to the near infrared, down to 1400 nm. The role of Au sulfidization in modifying the dynamics of Au NPs and of the corresponding plasmon resonance is discussed. The tunability of the plasmon resonance in a broad range is shown and the effectiveness as substrates for NIR SERS is demonstrated. The SERS response is investigated by using different laser sources operating both in the visible and in the NIR. SERS mapping of the SERS enhancement factor is carried out in order to evaluate their effectiveness, stability, and reproducibility as NIR SERS substrates, also in comparison with gold NPs fabricated by conventional sputtering and with the state-of-the-art in the current literature.

1. Introduction

Among the many promising applications of plasmonic gold nanoparticles (NPs), which span from photonic,[1] to photovoltaic,[2] bio-labelling,[3] and biosensing[4] uses, surface enhanced Raman scattering (SERS)[5] represents a reliable routine spectroscopic analytical tool concretely used nowadays. The high sensitivity of this technique in the selective detection of species in the proximity of the surface of plasmonic structures is commonly attributed to two main mechanisms. The first one is known as the chemical mechanism and is based on the enlargement of the molecules' Raman cross-sections due to their interaction with the metal,[6] as a consequence of the molecular adsorption onto specific sites when resonant charge transfer (CT) occurs. The second mechanism, known as the electromagnetic mechanism,[6] consists in the magnification of both incoming and Raman-scattered light due to their coupling with the collective excitations of the NPs conduction electrons, known as surface plasmons resonance (SPR). This electromagnetic effect reaches its maximum when the incident laser light frequency matches the SPR one.[7] Supported gold nanostructures are interesting as SERS substrates because they can accomplish plasmon resonance both in the near infrared (NIR) and visible range, matching standard laser sources for Raman analysis. Visible excitation laser sources commonly used in SERS experiments can cause photochemical reactions on the surface as well as fluorescence from the adsorbed molecules. A way to circumvent degeneration processes, avoid photochemical reactions and reduce analyte fluorescence is the use of laser sources in the NIR spectral range, where biomatter and common semiconductors are transparent. NIR SERS is exploitable for in vivo biological studies. This motivates the current interest in NIR-SERS and in developing NIR plasmonic substrates for obtaining maximum enhancement of Raman signals. To date, a common method to obtain SERS substrates with gold nanoparticles (NPs) exploits their colloidal chemical synthesis followed by self-assembling of NPs on substrates.[8] The progress achieved in chemical synthesis allows a plethora of gold NP shapes (i.e., triangles,[9] rods,[10] cubes,[11] prisms,[12] etc.) and structures (i.e., gold nanoshells[13] and nanocages[14]) with controllable size yielding tunable SPRs ranging from the visible to the mid-IR regions of the electromagnetic spectrum. The main problem with colloidal particles is their poor reproducibility when interacting with substrates because of the many factors that can affect their collective plasmonic behaviour,[6] which include NP overlapping electric field,[15] NP orientation on the surface and contact area,[16] and substrate polarizability and surface charge.[17] Moreover, both the synthesis and the assembly process of NPs require capping agents to ensure their stability in solution and their anchoring on the substrate. These can change the local dielectric environment of the NPs, influencing their resonance response and also preventing analyte adsorption on their surface. Differently, nanolithography and template-guided techniques enable the assembly of gold NPs of definite size and geometry and at predefinite locations and, therefore, a better definition of their collective plasmonic behavior.[18] Nanosphere lithography has been used to fabricate arrays of silver and gold NPs with controllable size, shape, and

Dr. G. V. Bianco, Dr. M. M. Giangregorio, Dr. M. Losurdo, Prof. P. Capezzuto, Dr. G. Bruno
Institute of Inorganic Methodologies and Plasmas (IMIP)-CNR
University of Bari
via Orabona 4, 70126 Bari, Italy
E-mail: giuseppevalerio.bianco@cnr.it; giovanni.bruno@ba.imip.cnr.it

DOI: 10.1002/adfm.201201441

interparticle spacing by using a close-packed monolayer of nanospheres as a metal deposition mask.[19] These techniques have the advantages of better reproducibility and the possibility to control the gap between nanoparticles. This is important because it has been demonstrated that the hot spots in the sub-nanometers gaps of large (over 50 nm) Au NPs can provide a SERS enhancement factor (EF) of 10^8 in a wide range of frequencies.[20] The shortcoming of these techniques is that the fabrication procedure is very complicated, with higher fabrication cost than the self-assembly techniques. Other attractive methods for the preparation of supported gold NP ensembles as SERS substrates are template-less physical vapor deposition (PVD) techniques, such as evaporation, pulsed-laser deposition,[21] and sputtering.[22] These dry approaches enable tunability of gold NP plasmonic properties in a narrower spectral range compared to the others cited above. Indeed, PVD self-assembling methodologies present desirable characteristics of compatibility with large area substrates, low cost, and, consequently, the advantage for a potential scaling-up to large-scale production. Therefore, developing cost-effective methodologies for the fabrication of reproducible SERS substrates is a very active field of research since the definition of a "best" SERS substrate is not univocal but depends on specific analytical and/or technical needs.

Here we demonstrate a novel template-less dry methodology for fabricating SERS substrates consisting of Au NP ensembles directly supported on crystal silicon (c-Si) with SPR ranging from the visible to the NIR. This methodology consists in two steps of Au PVD with a plasma-chemical treatment in between them: in the first step, Au NP seeds are created by sputtering a few Au monolayers and are thermally annealed; subsequently, a SF_6 plasma treatment is applied; finally, a second Au sputtering step is performed to enlarge the preformed Au seeds. In this way, we exploit surface chemical modifications by sulfidization of NP seeds to tailor NP growth dynamics, structure, and plasmonic behavior down to the NIR. Although polyhedral faceted Au nanoparticles have been synthetised by several groups using wet chemical routes,[23] our dry methodology represents the first attempt, to the best of our knowledge, of direct growth of substrate-supported faceted Au NPs without any capping and stabilizing agent by a dry, clean method. This is an important aspect also to fabricate SERS substrates with a clean surface to be used in SERS detection of molecule with a very low binding activity to substrates.

We demonstrate the feasibility of this methodology for engineering reproducible, large area, and stable SERS substrates with a tunable NIR-Vis resonance able to match NIR-Vis lasers wavelengths to gain high enhancement factors. Specifically, we tested the SERS efficiency of this plasmonic platform at different excitation wavelengths, both in the visible and in the NIR, also in comparison with conventional gold NPs. Real time spectroscopic investigation of the plasmon resonance during the growth process provides insights into the growth mechanism of these faceted NPs. Estimation and SERS mapping of the enhancement factor (EF) and benchmarking against other SERS substrates reported in the literature has been carried out to prove the effectiveness, stability, and reproducibility as NIR SERS substrates of supported Au NPs fabricated by this new PVD methodology.

2. Results and Discussion

The procedure for the NP growth on silicon substrate with SF_6 plasma is schematically described in **Figure 1**, where the simple direct sputtering method is also sketched for comparison. The deposited Au amount is controlled by the sputtering time, being known the deposition rate (approximately 0.1 Au ML s^{-1}, where ML = monolayer). The seed distribution (i.e., Au nuclei size and density) is tailored by the Au MLs deposited in the first sputtering step and by subsequent annealing time (in the range 10–60 min) and temperature (in the range 150–350 °C). Since PVD processes are usually carried out under conditions of supersaturation of vapor phase, the NP critical radius size is very small and the nucleation rate is high.[24] Thus, thermal annealing leads to the dissolution of Au particle nuclei with higher energy content into more stable particles by inducing coarsening and coalescence processes.[24] Then, Au seeds are exposed to SF_6 plasma to modify the surface chemistry of the silicon substrate as well as to form a thin shell of Au–S on the

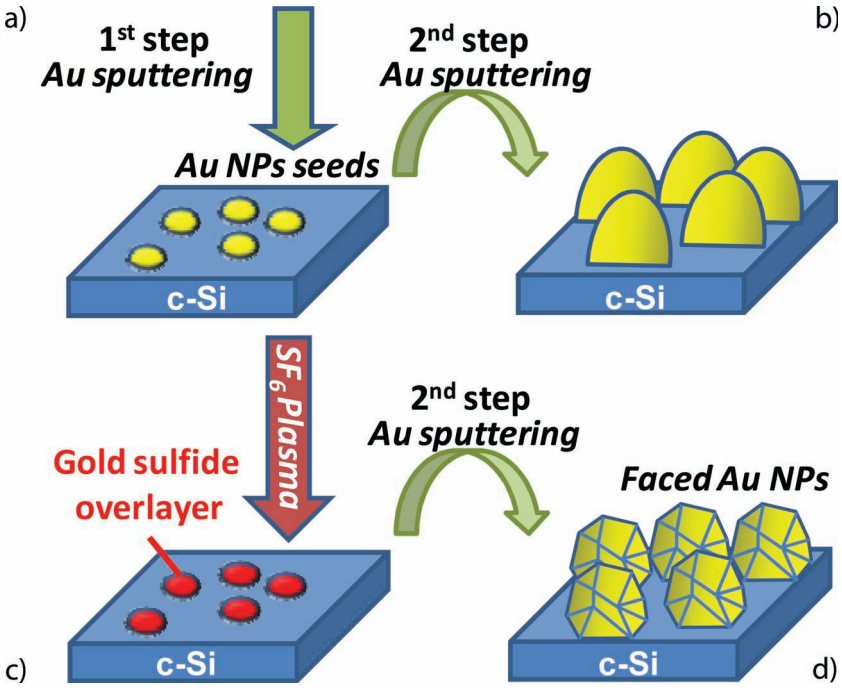

Figure 1. Schematic representation of the dry methodology for the growth of Au NPs with (a-c-d) and without (a,b) plasma chemical seeding: a) Au sputtering to nucleate metal seeds; b,d) second sputtering step to tailor NPs size; c) plasma treatment for the surface chemical modification of NPs seeds.

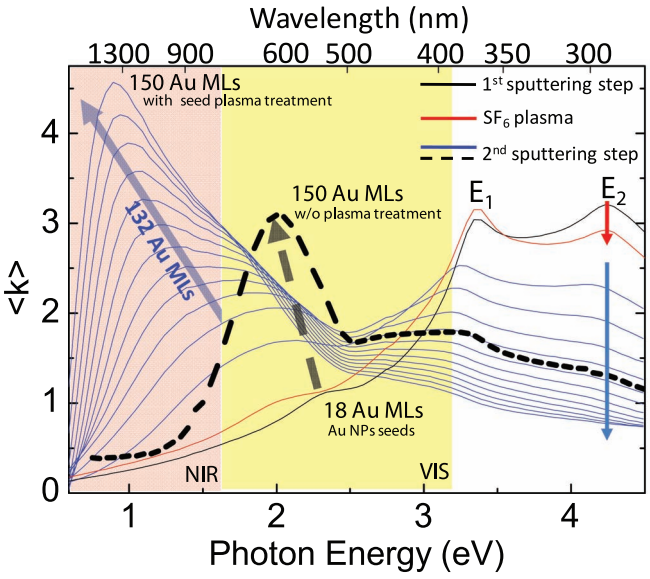

Figure 2. Real-time ellipsometric spectra of the pseudoextinction coefficient of the Au NPs supported on c-Si acquired in situ during the different stages of their growth: after the first sputtering of 18 Au MLs and annealing at 150 °C (black line); after SF_6 plasma treatment at 60 °C (red line); after each deposition of 11 Au MLs in the second sputtering step at 350 °C (blue lines). For comparison, the spectrum of Au NPs deposited under the same experimental conditions without seed plasma treatment is also reported (black dashed line).

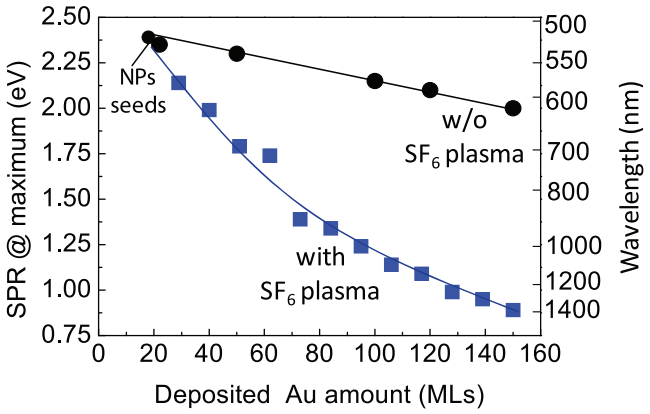

Figure 3. Evolution of the SPR peak with the increase in the deposited Au amount for NPs deposited with (blue dots) and without (black dots) SF_6 plasma treatment of the NP seeds.

seeds surface and/or to transform them into Au_2S seeds (as discussed below), both affecting the further nucleation of NPs as well as the growth of preformed seeds. These sulfidized seeds are exposed to a second Au sputtering step to tailor the final size and shape of the Au NPs, and therefore, their plasmon resonance.

During NP growth, the evolution of their plasmon resonance is monitored in real time using in situ spectroscopic ellipsometry (SE),[25] which provides a direct tool to tune the Au NP/c-Si plasmon resonance to a desired photon energy independently of knowing the NP structure or distribution. Real-time data also allow understanding of the growth kinetics of Au NPs in relation to their structural change. **Figure 2** shows the pseudoextinction coefficient spectra of the Au NP ensemble on Si acquired during the various deposition steps. In the spectral region above 3 eV, SE spectra are characterized by the E_1 and E_2 critical points (CPs) of c-Si,[26] whose amplitude decreases with the increase in the deposited Au MLs; therefore the analysis of this region is used to estimate the ML coverage by gold. Below 3 eV, spectra are characterized by the SPR peak of the Au NP ensemble, whose energy redshifts and amplitude increases by increasing the deposited Au MLs. Upon deposition of 18 MLs of Au, a SPR peak emerges at 2.38 eV (521 nm), which results from incident photons coupling into plasmon modes of the Au NP seeds. Upon SF_6 plasma treatment, the SPR energy redshifts to 1.9 eV because of the formation of a shell of Au–S (see below). During the 2nd sputtering step (blue curves in Figure 2) the SPR gradually redshifts from the visible to the NIR because of the increase in average NP size. For comparison, Figure 2 also shows the pseudoextinction coefficient spectrum of the NP ensemble produced by depositing an equivalent amount of Au sputtered conventionally without any SF_6 plasma treatment. While conventional sputtering yields NP ensembles with a symmetric SPR at approximately 620 nm, the stepwise SF_6 plasma treatment of NP seeds leads to a more intense resonance peak in the NIR (approximately 1400 nm), which clearly shows the contribution of different resonance modes. The NIR tunability of the SPR for the SF_6 treated NPs can also be seen in **Figure 3**, where clearly a faster SPR redshifting dynamic is found in comparison to the conventional sputtering for the same amount of deposited Au. Therefore, the SF_6 treatment of the Au NPs redshifts the SPR down to the NIR, whereas the conventional sputtering does not allow the amount of gold to redshift continuously the Au SPR, because of the coalescence of the NPs into a film; thus, only a slight redshift of almost 100 nm is observed by increasing the diameter of NPs.

The AFM phase images of the two Au NP/c-Si plasmonic systems produced with a total of 150 MLs of deposited gold are compared in **Figure 4**, together with their NP line profiles. No significant difference in particle density, lateral size, and height is seen from the line profiles that could explain the different plasmonic behavior. Indeed, upon SF_6 plasma treatment, NPs with sharp edges and terraces form, as opposed to the smooth Au NPs grown without plasma treatment. The faceted morphology of the stepwise grown particles is highlighted by the SEM images in Figure 4d. Therefore, the shift to the NIR of the SPR peak stems from the faceting of NPs produced by the SF_6 treatment.

The achieved size of the NPs in the range 50–100 nm is also interesting, since the use of large NPs promises a significant boost in SERS performance,[27] because such NPs have larger absorption and scattering cross-sections.[28]

In order to understand the change in the NP growth dynamics introduced by the SF_6 plasma, it has to be considered that in the conventional sputtering process, Au NP shape is mainly determined by minimization of surface area and energy.[24] This restricts NP plasmon resonance tunability mainly to variation of their size, since, by increasing their volume, the dephasing and retardation effect in electron plasmons move the resonance to smaller frequencies.[29] Indeed,

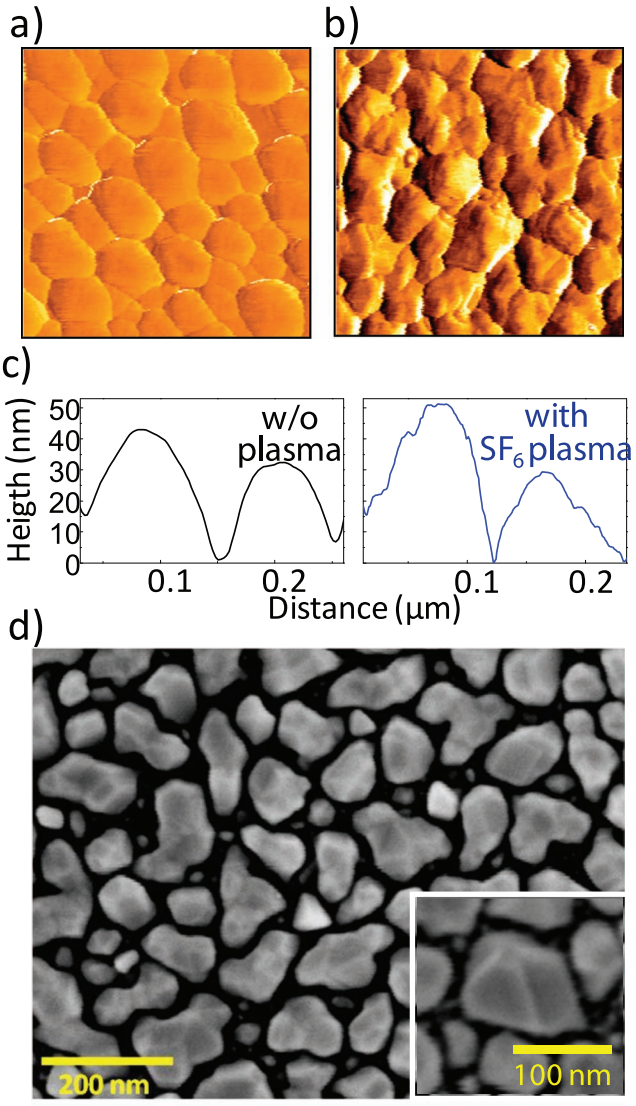

Figure 4. 500 nm × 500 nm AFM phase images of Au NPs/c-Si plasmonic systems produced by depositing 150 Au MLs with (b) and without (b) an SF_6 plasma treatment of NP seeds (18 MLs);and, c) relative NPs line profiles. d) SEM images of the Au NPs/c-Si plasmonic systems produced by depositing 150 Au MLs with SF_6 plasma treatment of the NP seeds

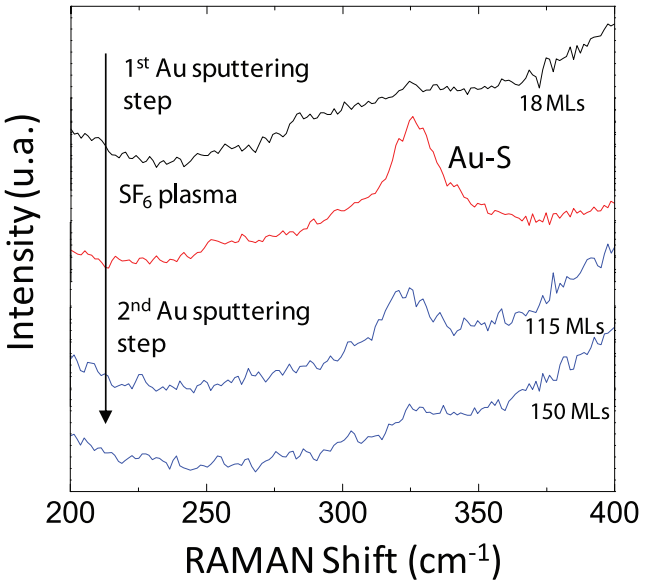

Figure 5. Raman spectra of Au NP seeds deposited in the first sputtering step (18 Au MLs), before (black line) and after (red line) SF_6 plasma treatment, and of Au NPs produced by depositing a total Au amount of 115 and 150 MLs.

this also enhances SPR broadening and, at last, suppression of the SPR band. Furthermore, for the conventional sputtering, there is a critical size above which the complete particles' coalescence into a continuous film occurs. Thus, it is not possible to continuously redshift the plasmon resonance by simply increasing the deposited Au amount. Conversely, the formation of edges, vertices and facets on the NPs affects the electrostatic distribution of the charges in the NP volumes,[16,30] leading to the generation of different multipolar moments and associated plasmon modes. For instance, in the case of Au NPs with polyhedral shapes (cubes, triangles, decahedron, etc.), multiple SPR absorbtion bands have been established in terms of their geometrical parameters,[3,16,30] providing tunability in a wider energy range with their dimensions.[31] The formation of gold NPs with a sharp surface faceting (Figure 4d) allows the exploitation of these multiple resonance modes. This explains the presence of distinct maxima in their plasmon band and their different size dependence. However, the presence of several SPR bands could also arise from the Au–S seed/Au core–shell structure because of the distinct SPR bands arising from the internal and external Au shell surfaces and their coupling.

This faceted growth dynamic relates to the SF_6 plasma-chemical treatment of the NPs seeds, forming a gold sulfide shell on NPs, as confirmed by the Raman spectra in **Figure 5**, showing a Raman band around 325 cm^{-1}, which can be attributed to the Au–S stretching mode.[32,33] This Au–S interlayer, which forms because of the strong affinity between the plasma generated sulfur atoms and gold, is within the Au NPs confined at the interface between the first and second Au sputtering steps, since it decreases in intensity with particle size increase. Despite numerous studies proposing the positions of Au atoms being essentially unperturbed upon atomic sulfur interaction and sulfur adlayer formation,[34] a dynamic surface restructuring and formation of gold sulfide phase have been demonstrated in literature even by sulfur adsorbed from gaseous SO_2.[35,36]

The faceted Au NPs originate from preferential nucleation and growth of Au along the gold-rich facets of gold sulfide seeds. This is because the (110) plane of the gold sulfide structure only contains gold atoms allowing preferential formation of Au–Au bonds at the interface with the Au–S seeds during the 2nd sputtering step, therefore, re-orienting growth of NPs. Specifically, the following orientation relationship:

$$(110)_{Au} \,//\, (110)_{Au_2} s; [1\bar{1}1]_{Au} \,//\, [1\bar{1}1]_{Au_2} s \quad (1)$$

has been reported for growth of Au on an Au–S phase.[31,37]

These faceted Au NPs have been tested as SERS substrate for the NIR. The SERS response of these plasmonic substrates has

been studied with three different laser wavelengths commonly found in Raman spectrometry: 532 nm (green), 633 nm (red), and 784 nm (NIR).

A conjugated rigid thiol has been used as the SERS probe molecule, the 4-methoxy-terphenyl-4''-methanethiol (TPMT). The presence of an aliphatic chain between the sulfur atom and the rigid aromatic system of this thiol allows its chemisorbtion on the gold surface (via Au–thiolate complexation through loss of hydrogen on the S–H group) by adopting a perpendicular orientation.[38] This yields very dense, and reproducible self-assembled monolayers, SAMs, on gold NPs. The NIR-SERS substrate presents a broader plasmon peak centered approximately around the used NIR laser wavelength (784 nm) and showing two distinct maximum at 684 and 886 nm (**Figure 6**c). For comparison, two SERS substrates providing plasmon resonances in the visible, respectively at 577 and 620 nm (Figure 6a,b) have also been prepared by sputtering of, respectively, 40 and 150 ML of Au. This allows direct correlation between the engineered NPs' plasmonic properties, the used excitation wavelength, and observed SERS signal intensities. SERS substrates spectra after thiol SAM formation are also reported in the figures. The thiol SAM functionalization of Au NPs results in a redshift of the SPR peak, being the plasmon resonance condition dependent on the dielectric properties of the NPs' local environment (including substrate, solvent, and adsorbates). According to the Mie,theory,[39] the resonance condition occurs when:

$$\varepsilon_1 = -2\varepsilon_m \quad (2)$$

Where ε_1 is the real part of the gold dielectric function and ε_m is the dielectric constant of the medium surrounding the particle. In the visible-NIR region, the negative real part of the dielectric constant increases with increasing wavelength. Therefore, an increase in the dielectric constant of the NPs' surrounding medium (or refractive index, $n_m = \varepsilon_m^{1/2}$, from $n_{air} = 1$ to $n_{sam} \approx 1.5$) is reflected as a red shift in the SPR band. The achieved SAM formation can also be inferred by the amplitude decreases of the E_1 and E_2 critical points of c-Si, which are very sensitive to the thickness of the overlayer.

SERS spectra of TPMT are reported in Figures 6d–n providing a matrix correlating the laser excitation wavelengths with the plasmon resonance wavelength. Typical features of the TPMT Raman modes can be recognized in each spectra and their detailed assignment can be found in a previous publication.[38] Figure 6 clearly shows the expected decrease of fluorescence band in the spectra with the increasing excitation laser wavelength, therefore confirming the advantage of moving the plasmon resonance in the NIR. Moreover, for each excitation source, the more the substrate plasmon peak matches the laser wavelength, the more intense is the recorded Raman signal, confirming the general "rule of thumb" of SERS.

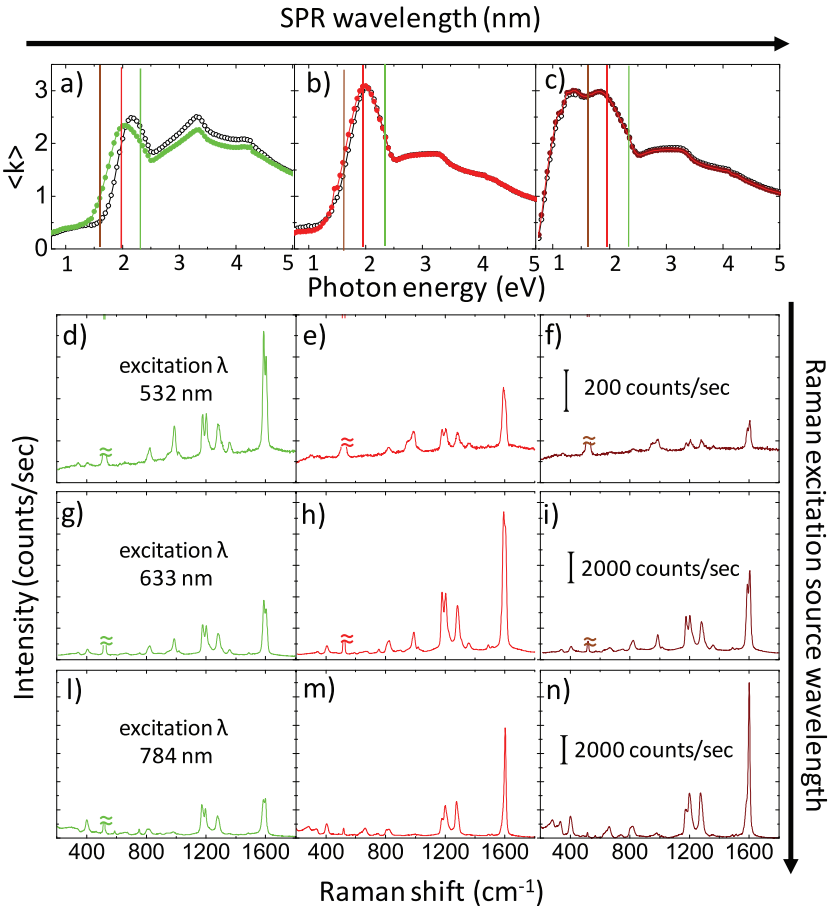

Figure 6. SE spectra (black lines) of Au NPs supported on c-Si fabricated by depositing, in the first sputtering step, 18Au ML, and, in the second one, respectively, a) 22,and, b) 132 Au ML (without any seed plasma treatment), and, c) 77 Au ML (on SF_6 plasma-treated seeds). Spectra after TPMT SAM formation are also reported (green, red, and brown lines, respectively, in a, b, and c). Vertical lines in a, b, and c indicate the energy of the irradiation source used (green = 532 nm, red = 633 nm, and brown = 784 nm). Relative SERS spectra of TPMT acquired with: d,e,f) 532 nm; g,h,i)633 nm; and l,m,n) 784 nm laser sources. For each laser source, SERS spectra are reported at the same scale. The c-Si Raman band in the spectra (≈) has been cut to highlight only thiol Raman modes.

We also provide an estimation of SERS enhancement achieved by each substrate with the different laser excitation sources by calculating the enhancement factor (EF). This is commonly defined as the ratio between the SERS and Raman signal intensities, I_{SERS} and I_{Raman}, recorded under identical experimental conditions, both normalized for the number of probed molecules, N_{SERS} and N_{Raman}:

$$EF = (I_{SERS}/N_{SERS})/(I_{Raman}/N_{Raman}) \quad (3)$$

Such an estimation must rigorously take into account all factors affecting SERS signal, including the laser source, the irradiation power, the substrate area, as well as the analyte's SERS cross-section and electronic resonance effects.[30] The EF values reported in the literature for different SERS systems are not always directly comparable. Indeed, the difficult estimation of

N_{SERS} and N_{Raman} parameters involves taking into account different approximations specific to the investigated SERS systems. In our case, N_{SERS} has been calculated by considering the focal beam diameter, the SERS active area of gold NPs (approximated by an ordinary geometric model described in the Experimental Section), and the surface packing density of the TPMT SAM[40] (arbitrarily considered uniform along all the NPs' surface area). Reference Raman spectra were acquired from a 1.0 M solution of TPMT in dichloromethane, deposited by drop-casting on c-Si substrate. Knowing the TPMT concentration in the solution, N_{Raman} was estimated by evaluating its irradiated volume for each laser wavelength. Although this approach is commonly used in the literature, it is, probably, the most problematic for estimating the EF. In fact, this involves the comparison of scattering signals originating from a 2D structure to that of a 3D volume and it arbitrarily neglects the non-uniform excitation and collection efficiency along the irradiation beam axis in the solution volume.

Thus, according to the specified approximations, EF has been calculated considering the intensity of the aromatic ring skeletal vibration peak, near 1600 cm^{-1}, which is the most intense peak in the TPMT spectra.

Average EF values and relative standard deviation as a function of the substrate plasmon peak and probing laser wavelength are reported in **Figure 7**. An important error in the determination of EF stems from uncertainity in the total surface coverage. We have computed that our area coverage values could be in error by a factor of two, as discussed in the literature.[41] Therefore, we have reported the minimum and maximum EF values for the 633 and 784 nm lasers (see shadow area in Figure 7). EF data show that an average enhancement as high as 9.8×10^4 is achieved when the substrate plasmon peak is in the nearest proximity of incoming light wavelengths. In the same figure, the highest EF values reported by others, who also declared the wavelength of the SPR, measured using the 784 nm laser, are also shown for comparison.

It can also be seen in Figure 7a that the EF values are two order of magnitude lower when irradiated with the green laser (532 nm) than with the ones operating at longer wavelengths. This agrees with experimental results reported by Lee et al[5] on the EF estimation of supported gold NP SERS substrates. They discussed the observed EF trend by considering that the NPs' plasmonic enhancement of Raman scattering became more important with the increase of the absolute value of the ratio between real and imaginary parts of the dielectric function of the metal, $|\varepsilon_1/\varepsilon_2|$. In the case of gold, indeed, this ratio increases steeply for wavelengths longer than 532 nm. In a simpler way, the lower magnitude in EFs achieved with the laser operating at 532 can be also explained by considering the contribution of the gold interband transition to the ratio of scattering to adsorption from photons interacting with NPS surface.[30] Towards the red, this contribution decreases and is effectively minimized for longer wavelength. This also suggests that NPs fabricated by plasma-seeded growth for longer sputtering time and, therefore, with resonance located at longer wavelength, would provide higher SERS responses when matched with an appropriate laser source (such as a Nd:YAG laser operating at 1064 nm) because of the synergistic contributions of both a higher ratio of scattering to absorption and of a higher volume.

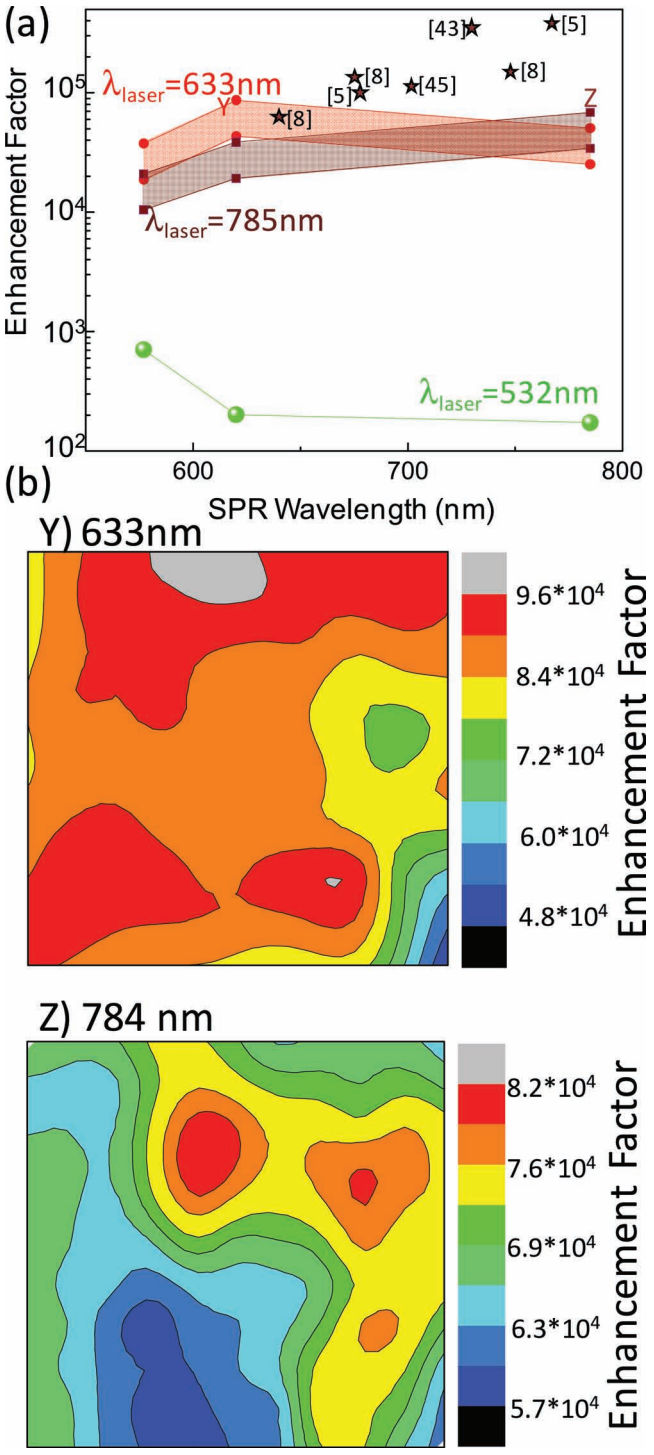

Figure 7. a) Average EF values as a function of the substrate plasmon peak and laser wavelength. For comparison, EF data from several references are also shown. b) 20 μm × 20 μm SERS maps of the EF acquired for the substrates Y and Z indicated in (a) with plasmon resonance around 620 and 784 nm probed with laser sources at 633 and 784 nm.

We evaluated the performance of our substrates by comparing them with a large variety of Au NP substrate categories, including defined nanoparticle cluster arrays and nonpatterned

substrates with a plasmon resonance in a similar range. As pointed out by the discussion below, our EF values of 4.5×10^4 to 9.8×10^4 fall within the typical SERS EF range of Au NPs films[42] and are comparable with those obtained by other engineered SERS substrates, such as Au nanoholes and nanodisks.[43] In addition to NP geometry, the interparticle gap is also an important parameter for EF. The increase of EF with decreasing NP gap is due to electromagnetic coupling between the NPs, which further increases the EF. An EF of 5.4×10^5 has been reported by Lee et al. for a NP gap of 4 nm, with the EF decreasing to 3.3×10^3 with the increase in gap size to approximately 20 nm obtained for self-assembled NPs guided by block polymer templates.[5] It has been reported that an EF in the range 1×10^6 to 4×10^6 can be obtained for nanoparticle cluster arrays of Au NPs, while for unpatterned NPs the EF is one order of magnitude lower, i.e., around 10^5, as in our case.[44] Fang et al.[41] also discussed and compared EF values in close-packed (CP) and non-close-packed (NCP) SERS Au NP substrates. They showed that for NCP substrates, as in the present case, 89% of points have EF in the range 10^4–10^5 with only 0.08% of regions having EF that can reach 10^8, while higher values of average EF of 4.2×10^5 with maximum in the 10^{10} range can be obtained for close-packed nanoparticles with gaps in the subnanometer. Furthermore, our EF is similar to the value of 1.1×10^5 for nanoparticle cluster arrays reported by Yan et al.[45] We also compare our EF also with those obtained by gold on polystyrene nanospheres, which is another approach used to gain high EF.[46] Baia et al. reported EF in the range 8×10^3 to 2×10^4 using the 633 nm laser, which is lower than our EF using the same 633 nm laser, while similar values to ours in the range 5×10^4 to 1×10^5 could be measured by the 784 nm laser. Finally, comparing our EF with that of other polyhedral Au nanocrystals obtained by a different methodology based on wet chemistry, Guo et al.[23b] reported a maximum EF of 6×10^4 at 1064 nm excitation. This comparison supports the suitability of our self-assembled faceted Au NPs compared to well-ordered structures or substrates obtained by templates.

Another aspect we addressed is the reproducibility and stability of our samples. One of the goals of nanofabrication is to create uniform EF substrates. Therefore, another important SERS characteristic is the reproducibility of EF over the substrate area. Additional information about EF distribution should be provided rather than ordinary measurement of EF alone.[41] Therefore, for each laser source and substrate used, we have recorded SERS signal 20 μm × 20 μm maps at different points on the samples and corrected by baseline subtraction to exclude the fluorescence contribution. The variability of EF is inferred from the maps shown in Figure 7b for the two samples with the highest EF at 633 and 784 nm. The variation of the EF in our case is 8% for the 784 nm laser and 9% for the 633 nm laser, which is below the values of 10% reported by Lee et al.,[5] and 12% reported by Yan et al.,[45] and much lower than the values of 40% for random colloidal substrates and 55% for nanopatterned disks.[45] Furthermore, both optical measurements for the plasmon resonance and SERS measurements after thiol functionalization were repeated many times at different points of the substrates and similar spectra, i.e., position and amplitude of SPR and of the Raman band, were obtained. In addition, the optical SPR and SERS measurements were repeated after several weeks and almost identical spectra were obtained, demonstrating the remarkable stability of the fabricated SERS substrates.

3. Conclusions

In summary, a stepwise PVD methodology to fabricate SERS substrate composed of self-assembled faceted supported Au NPs with plasmon resonance tunable in the range from 521 nm up to 1400 nm has been developed. This methodology exploits Au-sulfide seeds produced by a SF_6 plasma treatment of Au nuclei that are subsequently enlarged by a further sputtering steps, leading to multifaceted NPs with multiple plasmonic modes. The SERS response of this plasmonic platform has been tested and compared with that of conventional gold NPs fabricated by conventional one-step sputtering. SERS mapping of the enhancement factor has been carried out by using different laser sources operating both in the visible and in the NIR. Data have been discussed by considering the interaction of the incoming excitation wavelengths used with the specific optical and structural properties of each SERS substrate, as well as the intrinsic dielectric properties of gold NPs. SERS enhancement factor values in the range 4×10^4 to 1×10^5 have been measured. These values are very reproducible and with a very low standard deviation of 8%, as shown by maps of the EF. Thus, the large tunability of surface plasmon resonance combined with the advantage of relatively high average and reproducible EF demonstrate that supported gold NPs fabricated by this new PVD methodolology are effective, reproducible, and stable large area substrates for NIR SERS.

4. Experimental Section

Fabrication of SERS Substrates: Au NPs were deposited on native oxide-free c-Si (111) by sputtering an Au target using a radiofrequency (RF; 13.56 MHz) Ar plasma. The RF bias potential, pressure, and Ar flow rate were fixed at 500 V, 0.3 Torr, and 10 SCCM, respectively. The substrate temperatures during the first and second sputtering step were, respectively, 150 and 350 °C. In between sputtering steps, SF_6 plasma was carried out at the temperature of 60 °C for a time of 500 s. The RF power, pressure, and SF_6 flowrate were fixed at 50 W, 0.3 Torr, and 18 SCCM, respectively. The deposited Au amount was controlled by the sputtering time being known the deposition rate (approximately 0.1 Au ML s^{-1}, where ML = monolayer). The three probed SERS substrates were fabricated by depositing, in the first sputtering step, 18Au ML, and, in the second, respectively, 22 and 132 Au ML (without any seed plasma treatment), and 77 Au ML (on SF_6 plasma-treated seeds).

SAM Formation on Gold NPs: SAMs were formed by dipping substrates for 1 h in 1 mM solutions of TPMT in CH_2Cl_2 at 25 °C. Samples were subsequently rinsed with solutions solvents and dried under a N_2 stream.

Sample Characterization: Spectroscopic ellipsometry measurements of the pseudoextinction coefficient, $\langle k \rangle$, were performed in the range 0.6 to 4.5 eV using a phase-modulated spectroscopic ellipsometer (UVISEL-Jobin Yvon) at an incidence angle of 70°. Atomic force microscopy (AFM) was used for determining the morphological and geometrical characteristics of NPs using an AutoProbe CP Thermomicroscope in non-contact intermittent mode. SERS and Raman spectra were acquired with a Horiba Jobin-Yvon LabRAM HR-VIS microRaman spectrometer equipped with 532, 633, and 784 nm laser sources. A 50× objective (numerical aperture, NA = 0.75) was used for all of the measurements.

Incident laser powers of 45 mW (532 nm), 10 mW (633 nm), and 75 mW (784 nm), and acquisition time of 5 s were used for measurements. The number of molecules probed in the each SERS substrate, N_{SERS}, was calculated assuming that all the particles were perfect spherical caps with average base diameter, d, and height, h, derived from the AFM images and line profiles. For each probed SERS substrate, the resulting r and h were, respectively, 29 and 3 nm (SPR at 577 nm), 80 and 30 nm (SPR at 620 nm), and 35 and 11 nm (SPR around 784 nm). Due to the high NP distribution density (arbitrarily assumed to be uniform), the number of spherical caps in the irradiated substrate surface, N, was calculated as $N = A_{laser}/A_{NPs,}$ where A_{laser} is the laser spot area (πr_{laser}^2 with $r_{laser} = 0.61\lambda_{laser}/NA$), and A_{NPs} is the spherical cap base area. Each spherical cup surface, S_{NPs} was calculated as $2\pi Rh$ with $R = (((d/2)^2+h^2)/h)/2$. Thus, N_{SERS} was derived as the total NP area irradiated by the laser (derived as NS_{NPs}) divided by the TPMT SAM surface distribution density (8.0×10^{-10} mol cm^{-2} from reference[40]). N_{Raman} was derived by considering the irradiated TPMT solution volume (estimated as the product of A_{laser} and the laser spot depth of focus, $2\lambda/N{\cdot}A^2$) and its concentration (1.0 M).

Acknowledgements

This work was supported by the Regione Puglia through the "Reti di Laboratoio" project. It is our pleasure to acknowledge Cinzia Di Franco of CNR-IFN for SEM measurements, and Alessandra Operamolla and Homar Hassan Homar of CNR-ICCOM for the TPMT synthesis.

Received: May 29, 2012
Published online: August 7, 2012

[1] J. F. Galisteo-López, M. Ibisate, R. Sapienza, L. S. Froufe-Pérez, Á. Blanco, C. López, *Adv. Mater.* **2011**, *23*, 30.
[2] M. Losurdo, M. M. Giangregorio, G. V. Bianco, A. Sacchetti, P. Capezzuto, G. Bruno, *Sol. Energy Mater. Sol. Cells* **2009**, *93*, 1749.
[3] A. J. Haes, C. L. Haynes, A. D. McFarland, G. C. Schatz, R. P. Van Duyne, S. Zou, *MRS Bull.* **2005**, *30*, 368.
[4] J. N. Anker, W. P. Hall, O. Lyandres, N. C. Shah, J. Zhao, R. P. Van Duyne, *Nat. Mater.* **2008**, *7*, 442.
[5] W. Lee, S. Y. Lee, R. M. Briber, O. Rabin, *Adv. Funct. Mater* **2011**, *21*, 3424.
[6] S. Lal, S. Link, N. J. Halas, *Nat. Photonics* **2007**, *1*, 641.
[7] C. L. Haynes, R. P. Van Duyne, *J. Phys. Chem. B* **2003**, *107*, 7426.
[8] a) S. L. Smitha, K. G. Gopchandran, T. R. Ravindran, V. S. Prasad, *Nanotechnology* **2011**, *22*, 265705; b) B. Yan, A. Thubagere, W. R. Premasiri, L. D. Ziegler, L. Dal Negro, B. M. Reinhard, *ACS Nano* **2009**, *3*, 1190.
[9] J. E. Millstone, S. Park, K. L. Shuford, L. Qin, G. C. Schatz, C. A. Mirkin, *J. Am. Chem. Soc.* **2005**, *127*, 5312.
[10] X. Huang, I. H. El-Sayed, W. Qian, M. A. El-Sayed, *J. Am. Chem. Soc.* **2006**, *128*, 2115.
[11] S. Kundu, S. Panigrahi, S. Praharaj, S. Basu, S. K. Ghosh, A. Pal, T. Pal, *Nanotechnology* **2007**, *18*, 075712.
[12] J. E. Millstone, W. Wei, M. R. Jones, H. Yoo, C.A. Mirkin, *Nano Lett.* **2008**, *8*, 2526.
[13] J. B. Lassiter, M. W. Knight, N. A. Mirin, N. J. Halas, *Nano Lett.* **2009**, *9*, 4326.
[14] J. Chen, D. Wang, J. Xi, L. Au, A. Siekkinen, A. Warsen, Z. Y. Li, H. Zhang, Y. Xia, X. Li, *Nano Lett.* **2007**, *7*, 1318.
[15] W. Rechberger, A. Hohenau, A. Leitner, J. R. Krenn, B. Lamprecht, F. R. Aussenegg, *Opt. Commun.* **2003**, *220*, 137.
[16] C. Noguez, *J. Phys. Chem. C* **2007**, *111*, 3806.
[17] A. Pinchuk, A. Hilger, G. Plessen, U. Kreibig, *Nanotechnology* **2004**, *15*, 1890.
[18] N. Fèlidj, J. Aubard, G. Lèvi, J. R. Krenn, A. Hohenau, G. Schider, A. Leitner, F. R. Aussenegg, *Appl. Phys. Lett.* **2003**, *82*, 3095.
[19] L. A. Dick, A. D. McFarland, C. L. Haynes, R. P. Van Duyne, *J. Phys. Chem. B* **2002**, *106*, 853–860.
[20] K. L. Wustholz, A. I. Henry, J. M. McMahon, R. G. Freeman, N. Valley, M. E. Piotti, M. J. Natan, G. C. Schatz, R. P. V. Duyne, *J. Am. Chem. Soc.* **2010**, *132*, 10903.
[21] C. Domingo, V. Resta, S. Sanchez-Cortes, J. V. Garcia-Ramos, J. Gonzalo, *J. Phys. Chem. C* **2007**, *111*, 8149.
[22] A. Merlen, V. Gadenne, J. Romann, V. Chevallier, L. Patrone, J. C. Valmalette, *Nanotechnology* **2009**, *20*, 215705.
[23] a) A. Tao, P. Sinsermsuksakul, P. Yang, *Angew. Chem. Int. Ed.* **2006**, *45*, 4597; b) S. Guo, Y. Wang, E. Wang, *Nanotechnology* **2007**, *18*, 405602.
[24] a) C. V. Thompson, R. Carel, *Mater. Sci. Eng. B* **1995**, *32*, 211; b) C. V. Thompson, *Annu. Rev. Mater. Sci.* **2000**, *30*, 159.
[25] M. Losurdo, M. Bergmair, G. Bruno, D. Cattelan, C. Cobet, A. de Martino, K. Fleischer, Z. Dohcevic-Mitrovic, N. Esser, M. Galliet, R. Gajic, D. Hemzal, K. Hingerl, J. Humlicek, R. Ossikovski, Z. V. Popovic, O. Saxl, *J. Nanopart. Res.* **2009**, *11*, 1521.
[26] E. Aspnes, A. A. Studna, *Phys. Rev. B* **1983**, *27*, 985.
[27] P. N. Njoki, I. I. S. Lim, D. Mott, H. Y. Park, B. Khan, S. Mishra, R. Sujakumar, J. Luo, C. J. Zhong, *J. Phys. Chem. C* **2007**, *111*, 14664.
[28] A. Chen, A. E. De Prince, A. Demortiere, A. Joshi-Imre, E. V. Shevchenko, S. K. Gray, U. Welp, V. K. Vlasko-Vlasov, *Small* **2011**, *7*, 2365.
[29] S. S. Link, M. A. El-Sayed, *J. Phys. Chem. B* **1999**, *103*, 4212.
[30] S. A. Maier, *Plasmonics: Fundamentals And Applications*, Springer Science+Business Media LLC, **2007**, Ch. 5.
[31] M. Tréguer-Delapierre, J. Majimel, S. Mornet, E. Duguet, S. Ravaine, *Gold Bull.* **2008**, *41*, 195.
[32] Y. Fan, Y. F. Long, Y. F. Li, *Anal. Chim. Acta* **2009**, *653*, 207.
[33] G. K. Parker, K. M. Watlinga, G. A. Hopea, R. Wood, *Colloids Surf.,A* **2008**, *318*, 151.
[34] C. Vericat, J. N. Andersen, M. E. Vela, R. C. Salvarezza, *J. Phys. Chem. B* **2000**, *104*, 302.
[35] B. K. Min, A. R. Alemozafar, M. M. Biener, J. Biener, C. M. Friend, *Top. Catal.* **2005**, *36*, 77.
[36] M. M. Biener, J. Biener, C. M. Friend, *Surf. Sci.* **2007**, *601*, 1659.
[37] J. Majimel, D. Bacinello, E. Durand, F. Vallée, M. Tréguer-Delapierre, *Langmuir* **2008**, *24*, 4289.
[38] G. Bruno, F. Babudri, A. Operamolla, G. V. Bianco, M. Losurdo, M. M. Giangregorio, O. Hassan Omar, F. Mavelli, G. M. Farinola, P. Capezzuto, F. Naso, *Langmuir* **2010**, *26*, 8430.
[39] G. Mie, *Ann. Phys.* **1908**, *25*, 377.
[40] Y. Tao, C. Wu, J. Eu, W. Lin, *Langmuir* **1997**, *13*, 4018.
[41] Y. Fang, H. Yang, P. Jiang, D. D. Dlott, *J. Raman Spectrosc.* **2012**, *43*, 389.
[42] C. L. Haynes, A. D. McFarland, R. P. Van Duyne, *Anal. Chem.* **2005**, *77*, 338.
[43] Q. Yu, P. Guan, D. Qin, G. Golden, P. M. Wallace, *Nano Lett.* **2008**, *8*, 1923.
[44] L. Yang, B. Yan, W. Ranjith Premasiri, L. D. Ziegler, L. Dal Negro, B. M. Reinhard, *Adv. Funct. Mater.* **2010**, *20*, 2619.
[45] B. Yan, A. Thubagere, W. Ranjith Premasiri, L. D. Ziegler, L. Dal Negro, B. M. Reinhard, *ACS Nano* **2009**, *3*, 1190.
[46] L. Baia, M. Baia, J. Popp, S. Astilean, *J. Phys. Chem. B* **2006**, *110*, 23982–23986.